APPLICATION OF A 3D INVERSE CAMBER-LINE DESIGN METHOD FOR A HIGHLY-LOADED AXIAL-FLOW LOW-SPEED COMPRESSOR ROTOR

C. Clemen
Installation Aerodynamics, Rolls-Royce Deutschland Ltd. & Co. KG
Eschenweg 11, Dahlewitz, 15827 Blankenfelde-Mahlow, Germany
Carsten.Clemen@rolls-royce.com

V. Gümmer
Compressor Aerodynamics, Rolls-Royce Deutschland Ltd. & Co. KG

ABSTRACT

A new method for the three-dimensional design of blades for axial-flow compressors has been developed. This new method incorporates the systematic application of sweep and dihedral at hub and tip and introduces three-dimensional inversely calculated camber-lines for a prescribed three-dimensional load distribution into the blade design. The resulting blade shape matches the three-dimensional flow environment and achieves a large reduction in secondary losses. This can be achieved by significantly improving the rotor tip clearance flow and the rotor hub corner separations. With this improvement of the behavior of the secondary flow phenomena a considerable increase in rotor and stage efficiency as well as stability was obtained compared to modern conventionally designed blades. The new method has been applied to the design of a rotor for a highly-loaded single-stage axial-flow low-speed research compressor and was validated by means of 3D-Navier-Stokes calculations and experiments giving an increase in design point stage efficiency of 1.5% and a 20% improvement in stall range.

1 INTRODUCTION

The development of the design of recent axial compressors aims for increasing pressure ratio with decreasing number of stages. This requires an increased stage pressure ratio and therefore an increase in stage loading. But the increased loading results in larger secondary flows and higher losses, which have a negative impact on compressor stability and efficiency. Since the trend towards higher loaded compressors will be enforced, the recent designs come to their limits.

The idea on which the present work is based, is to account for means to reduce the losses in the early design phase. This is valid for the losses which occur on highly-loaded compressor blades on the fixed end (hub and/or casing) and the free end (hub or tip gap), generated by secondary flows like gap flow and gap vortex, horseshoe vortex, cross-passage flow and corner separations. At the same time also the regions of the blade where the primary (main) flow is responsible for the losses should be designed for minimum loss.

This can be achieved by changing the blade geometry systematically by the application of blade sweep and dihedral, profile stagger and camber of the individual profiles.

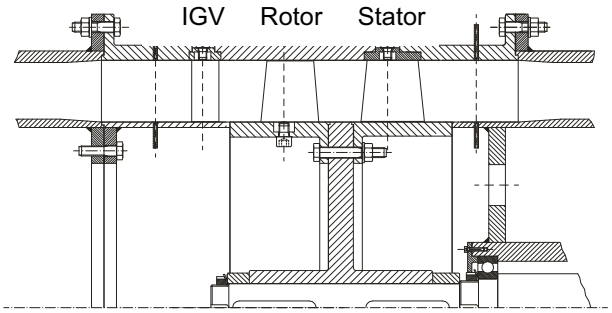

Figure 1: single-stage Braunschweig LSRC

This paper presents:

a) the features of a three-dimensional rotor design, which are the systematic application of sweep and dihedral at hub and tip and the inverse calculation of the radial camber-line distribution for a prescribed three-dimensional blade plan form and load distribution including a short description of the inverse design approach.
b) a comparison of the optimized design for the single-stage low-speed research compressor (LSRC) at the TU Braunschweig (Figure 1)

with a conventionally designed rotor blade with modern front loaded CDA camber lines.

c) results of the numerical and experimental investigation in terms of stage and rotor characteristics of both the 2D and the 3D configuration.

The TU Braunschweig LSRC has been designed in the EU-AdComB project such, that it is representative for the subsonic stages of a modern highly-loaded high-pressure compressor [1-5]. The main design parameters of the compressor are summarized in Table 1.

Compressor outer diameter	600 mm	Rotor tip *Mach* number	0.25
Compressor inner diameter	450 mm	mean rotor/stator diffusion factor	0.50
Hub-to-tip ratio	0.75	Corrected design mass flow	6.82 kg/s
Number of blade (Inlet guide vane, rotor, stator)	45 – 43 – 45	Corrected design speed	2800 rpm
Rotor/stator aspect ratio	1.0	Rotor/stator gap height	1.0 %

Table 1: Design parameters of the Braunschweig LSRC

2 3D ROTOR DESIGN

2.1 Sweep and dihedral

To determine and understand the qualitative influence of the blade parameters sweep and dihedral on the complex blade flow, it is necessary to develop a method, which allows to investigate isolated effects by varying the individual parameters seperately. This is not possible with known numerical 3D-methods used in industry today. These are iterative, very time consuming and require large computing resources.

Here a panel method is used [6], which is based on linear wing theory. This approach is suitable as long as the blade geometry and the inflow conditions fulfill the boundary conditions of the linearised potential equations. This means: small angle of attack, non-rotational flow, subsonic flow, small camber, linear dependency to the angle of attack and ideally an infinite aspect ratio. Such a method is able to calculate the inviscid three-dimensional load distribution. To make this method suitable for the application to compressor blades it has been developed further by *Clemen*, using previous investigations [7].

Since the application of sweep and dihedral on compressor blades is only reasonable near the endwalls the following modifications to the standard panel method are introduced:

- Mirroring the blade across beyond the endwall contour to simulate effects present at the mid section of a wing. On the opposite side the blade is enlarged towards infinity. So it is possible to determine the isolated effect of sweep and dihedral on the near wall sections without any influence of the opposite wall. If this influence is of interest, the results of calculations for each side can be superposed to the result of the finite blade.
- To account for the influence of a gap on one blade end, a simple gap model is introduced to calculate its potential effect on the load distribution of the blade and its interaction with sweep and dihedral.
- Since neither sweep and dihedral nor the chord length is constant along the height of compressor blades, the method has to be modified to cope with arbitrary blade plan forms.

Figure 2 shows the blade panel model taken from [8].

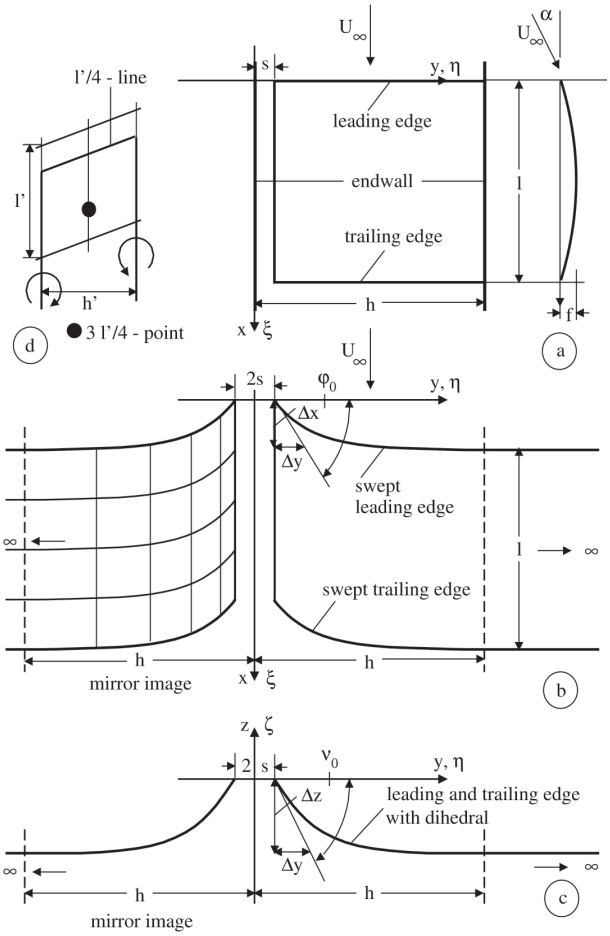

Figure 2: Semi-infinite single-blade model with mirror-image

A parameter study has been performed to investigate and understand the basic influence of sweep and dihedral on the blade loading distribution and to determine the optimum leading edge shape [9]. Based on those results sweep and dihedral are applied to define the plan form of the LSRC rotor.

The amount of positive sweep at the rotor tip is according to [8] set to 45° combined with an increased

tip chord length. The radial extension is limited to the upper third of the blade [8].

On the hub a positive sweep of similar amount and radial extension is applied with the aim to reduce the corner separation on the highly-loaded hub near blade sections.

Figure 3: Rotor blade

To reduce the hub corner separation further also a dihedral is applied. In [9] it has been shown, that on a rotor blade with 20° dihedral the loading at blade mid-height is increasing when the blade pressure ratio is maintained. This effect is not desired since it leads to higher profile loss. If the dihedral is larger than 30° the losses at mid-height can increase more than the losses are decreased at the hub [10] caused by an increase in the leading edge loading [8]. So a dihedral of 15° applied to the lower third of the blade is a good choice.

On the tip a dihedral of same amount and extension is aerodynamically sensible [11].

Figure 3 shows the rotor blade.

2.2 Inverse camber-line design

Based on the panel method mentioned above, which allows the calculation of the three-dimensional load distribution of a prescribed single blade with arbitrary blade plan form and geometry, a new method is developed, which calculates the camber-line distribution from a given three-dimensional load distribution and blade plan form. Hence this is an inverse design method.

Different to the method above, the inverse design method is not applied to a blade model of semi-infinite span and with a superposition for the finite blade and a correction for the cascade, but the real cascade geometry is considered for the calculation. This approach makes some changes necessary:

- The method uses finite blades of arbitrary plan form (Figure 4). This requires a suitable distribution of discrete panels on the blade.
- To account for the effects of the two end-walls, the blade is mirrored on the walls. Since the blade is finite, the mirroring has to be done not only once but as often as the blade model is extended to infinity to avoid any influence on the calculation by effects generated by a free blade end, Figure 4 a) and b).
- Besides the effects of the end-walls the influence of the cascade should be considered in the inverse calculation of the camber-line by modelling the real cascade geometry and not by a correction. This requires a duplication of the mirrored single blade models to a cascade, allowing for its geometry (stagger, spacing), Figure 4 c).
- A suitable duplication factor in y and z-direction, determined in a sensitivity study [7], is 20.
- By the mirroring of the geometry and its duplication to the cascade much more panels and control points are needed to discretize the geometry sufficiently as for the panel method in Figure 2. So the equation system, which has to be solved, gets much larger. This requires some simplifications:
    - The influence of the gap is not considered, since this is also not taken into account in today's blade design process based on S1- and S2-methods. So this is an acceptable simplification.
    - The panels are not overlayed with full horse-shoe vortices with lifting and non-lifting part but only with the lifting part of the bound vortex, Figure 4 a) and b). This means that the prescribed three-dimensional load distribution has to be constant in blade span-wise direction. This simplification is feasible, since for compressor blades a uniform distribution of the work along the blade height is intended. The disregard of the bound part of the non-lifting vortex leads to a certain inaccuracy of the method. But this is small and hence acceptable.
- The value, which has to be determined in the control points, is not the circulation, as in the method described above, but the induced velocity.

With the rotor plan form (stacking of the profile sections, chord length) the profiles of the blade sections are adjusted individually to the three-dimensional flow environment to minimise the losses in the design point.

As a constraint the thickness distribution of the reference rotor is maintained. Only the camber-lines are modified, since they influence the blade loading distribution most.

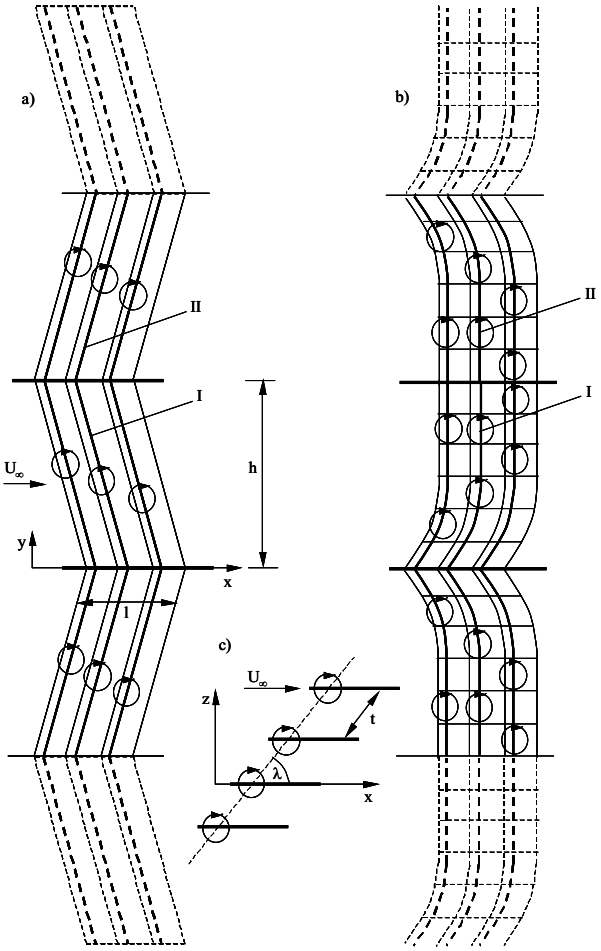

Figure 4: Inverse camber-line method

For the optimisation the blade is divided into three critical parts: hub, mid and tip with gap:

- On the lower third in the blade the secondary flow is determining the pressure loss. It is generated by the hub corner separation and the cross-passage flow.
- Between 35 % and 65 % blade height a two-dimensional flow can be approximately considered. The profile loss causes the biggest part of the overall loss.
- On the upper quarter the secondary flow by the gap flow and the gap vortex are critical for the losses.

These totally different phenomena require individual solutions, this means individual camber-lines for the different regions. With the application of the inverse camber-line they can be determined.

Tip

Close to the gap a uniform, ideally a constant, load distribution has to be achieved according to [12], since this generates lowest loss. Off-loading the front blade half causes a lower vortex strength and a less steep vortex trajectory. The larger pressure difference on the rear half causes a stronger flow through the gap, which stabilizes the vortex. This leads to higher efficiency and stability.

The boundary condition for the inverse camber-line method is a rectangular Δc_p on the blade sections above 90 % blade height and a triangular Δc_p below 65 % blade height, in between a smooth transition is applied.

The resulting profile for the tip section is depicted in Figure 5.

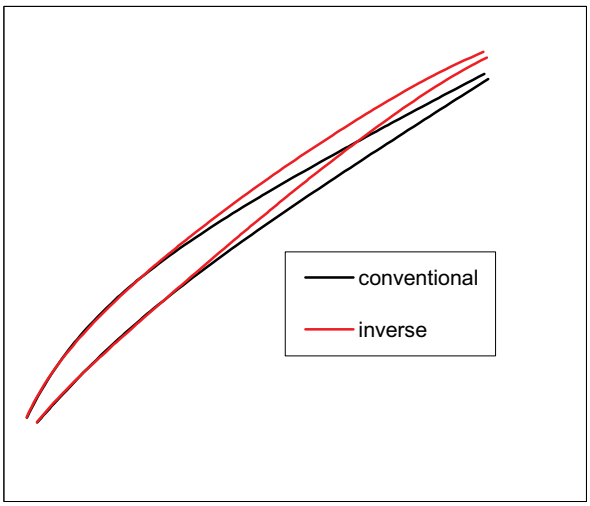

Figure 5: Inverse and conventional blade p rofile at 100 % blade height

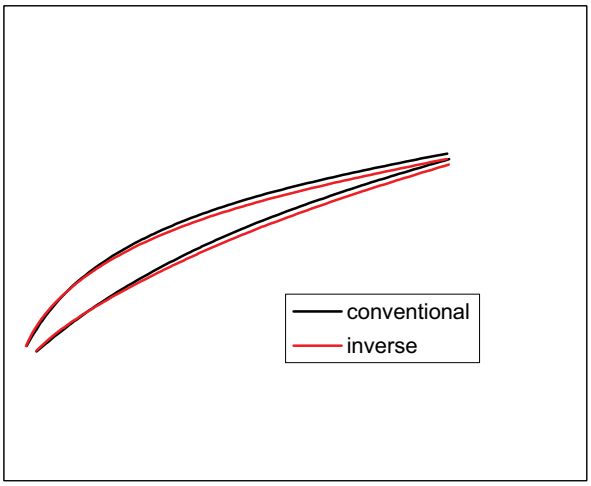

Figure 6: Inverse and conventional blade profile at 50 % blade height

Mid

Between 35 and 65 % blade height a camber-line distribution is required, which delivers the optimum distribution for an approximately two-dimensional flow.

This is theoretically according to *Stratford* [13] a triangular load distribution in terms of the pressure difference $\Delta c_p = p_{DS} - p_{SS}$ between pressure and suction side. This distribution has its pressure and *Mach* number peak at the leading edge and so the entire chord length is available for a smooth deceleration of the flow. This leads to minimum profile losses and maximum working

range. Practically this gives a strongly front loaded profile, see Figure 6.

Hub

For the hub sections a different approach has to be chosen. Here the aim is to reduce the corner separation. This can be achieved by off-loading the front half of the blade, this means by a shift of the loading downstream. A camber-line which fulfills that in combination with the positive hub sweep is a circular arc camber-line, compare [14] and [15]. This gives the hub profile shown in Figure 7.

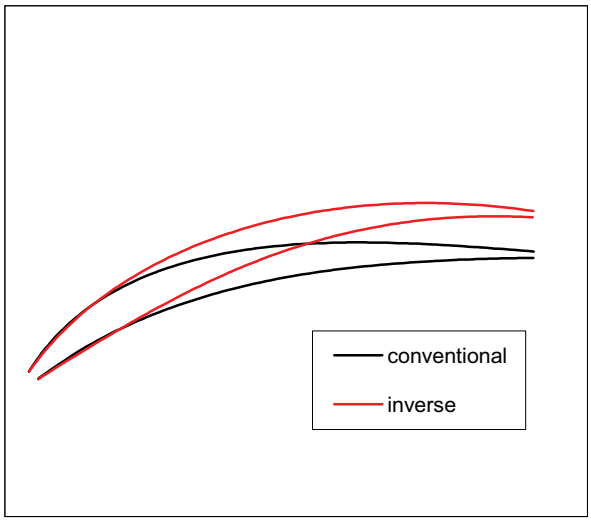

Figure 7: Inverse and conventional blade profile at 0 % blade height

3 SETUP OF CFD ANALYSIS

The numerical investigations are carried out with the 3D-RANS-CFD suite of NUMECA Fine/Turbo and the RR RANS code HYDRA. The turbulence models used are the *Baldwin-Lomax* and the *Spalart-Allmaras* models. In results presented in Chapter 5 are from Fine/Turbo with the *Baldwin-Lomax* turbulence model.

The calculation is carried out on structured grids with non-reflecting mixing planes between adjacent blade rows. The three blade rows are meshed with multi-block H-meshes (Figure 8 a)). The number of nodes used for the stage is approximately 800.000. Thereby about 94.000 cells are in the IGV domain, 294.400 cells are in the rotor domain and 337.600 cells are in the stator domain. Additionally the rotor and stator gap are meshed with so called „butterfly"-meshes – a combination of an H-mesh surrounded by an O-mesh, see Figure 8 b). In radial direction 13 cells are applied in the gaps. The mesh refinement has been optimised iteratively, further information can be found in [12], [3] and [4]. The wall distance has been set such, that the y^+ value is << 10 to fit the requirements of the turbulence models.

As inlet conditions the measured radial total pressure profile, the total temperature and the inlet whirl of the IGV are defined. The different operating points are set by a varying back-pressure. The last stable point in the CFD is considered as numerical stall margin.

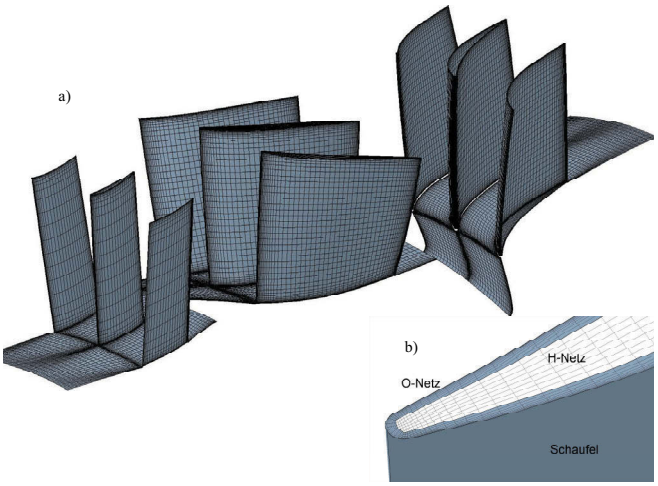

Figure 8: CFD grid

4 RIG AND TEST SETUP

The testing of the two-dimensional rotor was performed during the AdComB-project by *Rohkamm* [16]. The measurements of the three-dimensional rotor are performed within the scope of the present work.

4.1 Instrumentation

For the recording of the different measured variables, which are necessary for the analysis of the flow, the rig is equipped with a couple of measuring devices. The most important are depicted in Figure 9 and are shortly described. A more exact explanation of all details of the measuring equipment is given in [16]. Figure 9 shows five measuring planes (0, 1, 2, 3 und 3'), whose positioning is aligned to the hub leading edge point of the two-dimensional rotor.

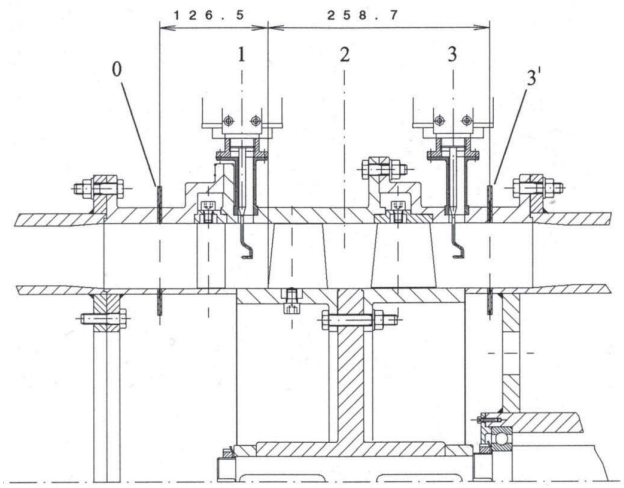

Figure 9: CFD grid Measurement planes in the LSRC

For the calculation of the stage static pressure ratio the static pressure at casing and hub about one chord upstream the inlet guide vane (measuring plane 0) and about one chord downstream the stator (measuring plane 3') is measured with twelve static pressure tappings each and is averaged using a settling chamber. The exact positions of the measuring planes can be taken from Figure 9. Following pressure differences are measured with inductive difference pressure devices with a measuring inaccuracy of ± 0.1 %:

- the pressure difference between inlet and outlet ($\Delta p_{3,0}$).
- the pressure difference between ambient and inlet plane ($\Delta p_{Umg,0}$)
- the pressure difference between ambient and the pressure in the intake duct (Δp_D)

The temperature measurements at inlet, exit and ambient are performed with Pt-100 resistance thermo-couples with a measuring inaccuracy of ± 0.5 K.

Besides the static pressures in the measuring plane 0 the inlet flow can be traversed with a total pressure probe. Together with the static pressure the velocity distributions at the inlet and the boundary layer behaviour can be determined.

Downstream of each blade row calibrated five-hole probes are positioned in the measuring planes 1, 2 and 3 at x = -24.8 mm, 87.8 mm and 217.0 mm. With these the radial traversing is done to determine the circumferentially averaged radial distributions of velocity and exit angle. The probes can be moved continuously with step motors over the duct height between 5 % and 97.5 %. Additionally in the measuring plane 2 a cylinder head probe is used for unsteady wake measurements, which also can be moved radially. The sampling of the flow field in circumferential direction is arranged such that the inlet guide vane and the stator can be rotated by an arbitrary angle relative to the probe.

The casing static pressure distributions over the rotor tip gap are determined with high frequency pressure sensors (Kulite XTE-190-25psi), which can be moved over the whole axial chord length of the rotor tip and which are rotatable in circumferential direction by 180°. Furthermore it is possible to visualise the flow over the rotor tip with oil film technique.

For the calculation of the efficiency, the reaction force F of the driving motor is measured with a DMS-force transducer (measuring range 200 N, accuracy class 0.1). The rotational speed of the compressor is adjusted with an electrical scanning and an electrical counter with a measuring accuracy of ± 0.1 %. The accuracy of the efficiency calculation is due to the above mentioned values to ± 1.8 % with a repeat accuracy of ± 0.4 %.

All measured variables are recorded, treated and stored with a measuring software.

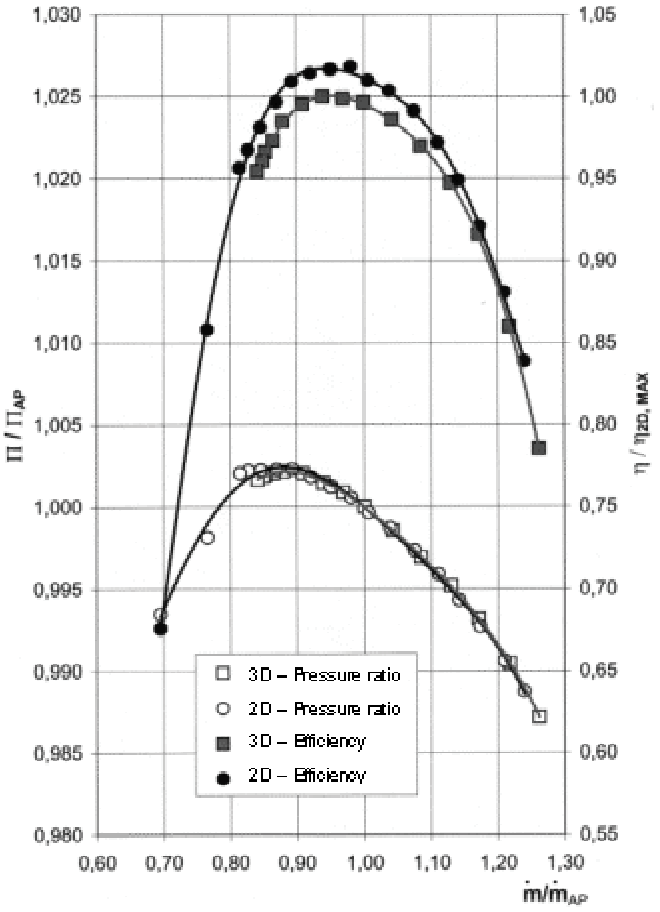

Figure 10: Measured stage characteristics of rotor 2D and 3D

5 CFD AND TEST RESULTS

5.1 Overall performance

Figure 10 shows the measured and Figure 11 the calculated characteristics of the stage with the conventional (2D) and the inverse designed (3D) rotor. At the same stage pressure ratio in the design point the 3D stage shows in the calculation in Figure 11 a 0.5 % higher efficiency than the 2D stage, the peak efficiency is even 0.85% higher. In the measurement (Figure 10) the improvement is even higher: 1.1 % at the design point and 1.6 % peak. Additionally it can be seen that the improvement of the efficiency is not only limited to flows smaller than the design point but for the whole operating range.

Regarding the stall margin (Equation 1) the improvement of the 3D versus the 2D rotor is higher in the calculation (+6 %, from 12 % to 18 %) than in the test (+4 %, from 19 % to 23 %). But it has to be kept in mind that the stall margin is by 6 % lower in the CFD for both stages than measured, since in the steady calculation a numerical stability limit is reached and not the aerodynamic stall margin.

Besides this difference, the qualitative agreement is good, whereby the measurement shows generally a higher improvement than the CFD.

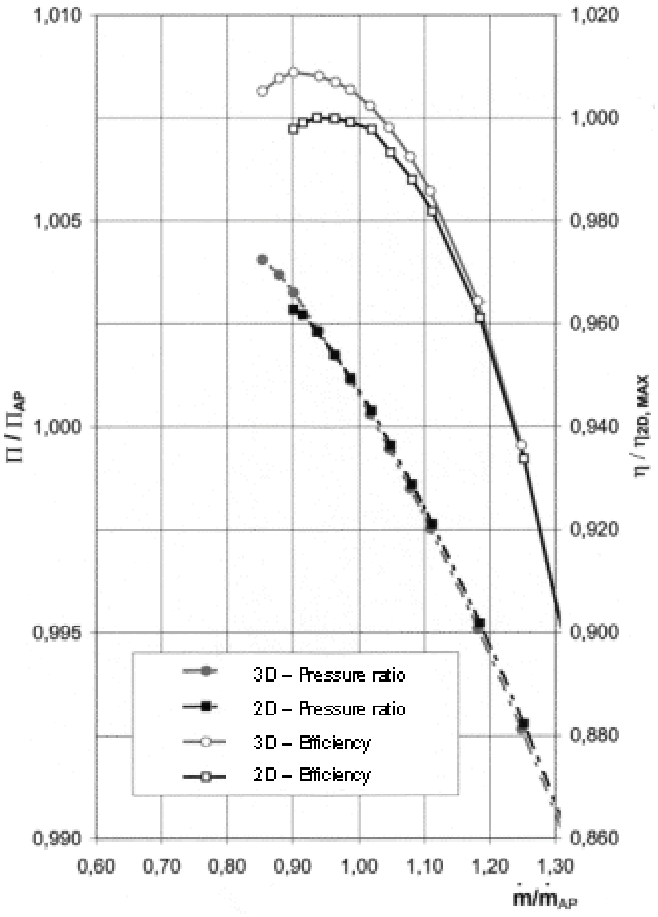

Figure 11: Calculated stage characteristics of rotor 2D and 3D

$$SM = \frac{\frac{\Pi}{\dot{m}_{SM}}}{\frac{\Pi}{\dot{m}_{DP}}} - 1 \qquad (1)$$

5.2 Circumferentially averaged parameters and flow field in the rotor wake

Although the stability in the calculation is limited numerically, the losses for rotor 2D and 3D for design and near stall point in Figure 12 clearly show that the stability is limited by the flow behavior at the rotor tip. When the compressor is throttled the loss on the rotor tip is increasing dramatically especially for rotor 2D. A comparison with rotor 3D shows, that this one has 8 % less local loss on the tip as a consequence of the inverse design. When the compressor is throttled rotor 3D loss stays below the rotor 2D loss at the design point.

Also on the hub the losses of rotor 3D are always significantly lower than that of rotor 2D caused by the introduction of sweep, dihedral and optimised camber-line. Only at mid-height the losses of the three-dimensional rotor are slightly higher than for the 2D rotor. Reason for that is the load re-distribution as a result of the dihedral at hub and tip. Nevertheless the overall losses of rotor 3D are significantly lower than for rotor 2D and hence the efficiency improvement can be explained.

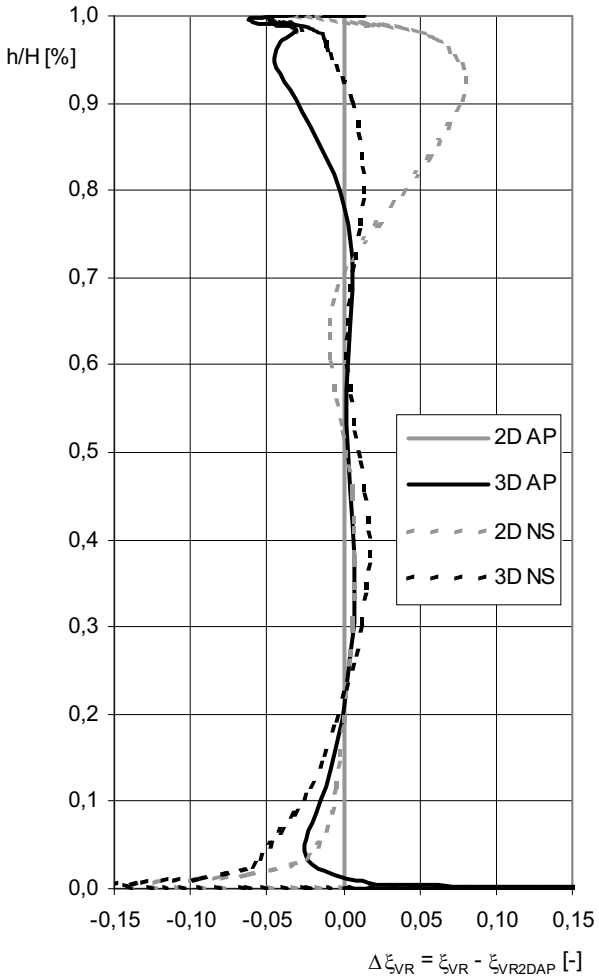

Figure 12: Calculated losses of rotors 2D and 3D at design point and near stall

An important criterion for the improvement of the losses of rotor 3D compared to rotor 2D can be identified when the circumferentially averaged absolute total pressure distribution in the rotor exit plane (measurement plane 2, Figure 9) is analysed. Figure 13 shows the total pressure for both rotors over duct height for the design point (AP) and the near stall point (NS). The pressure distribution of rotor 3D is characterised by an higher pressure level at the hub and at the tip. At mid-height the pressure is lower than for rotor 2D. This means that the total pressure profile of rotor 3D comes closer to the intended constant pressure profile along blade height due to the redistribution of the loading as a result of the improved flow conditions on the end-walls.

Therefore rotor 3D delivers improved inlet conditions for the downstream stator leading to the fact that the stage efficiency is increasing more than the rotor efficiency.

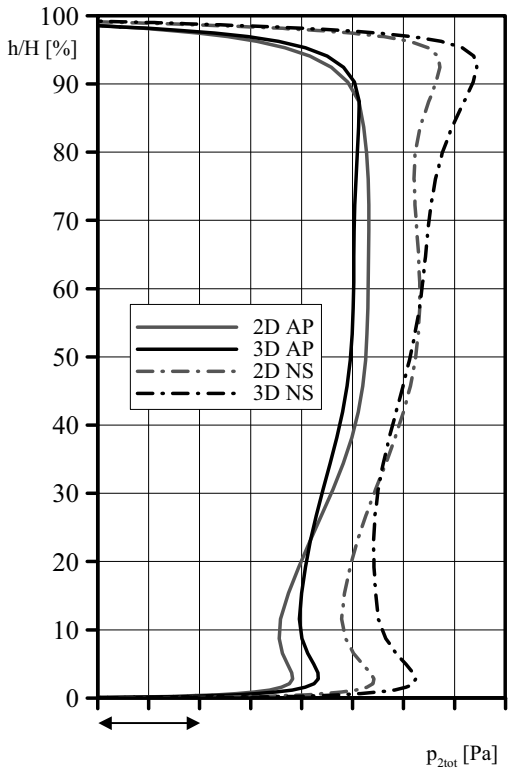

Figure 13: Calculated averaged absolute total pressures of rotors 2D and 3D at design point and near stall

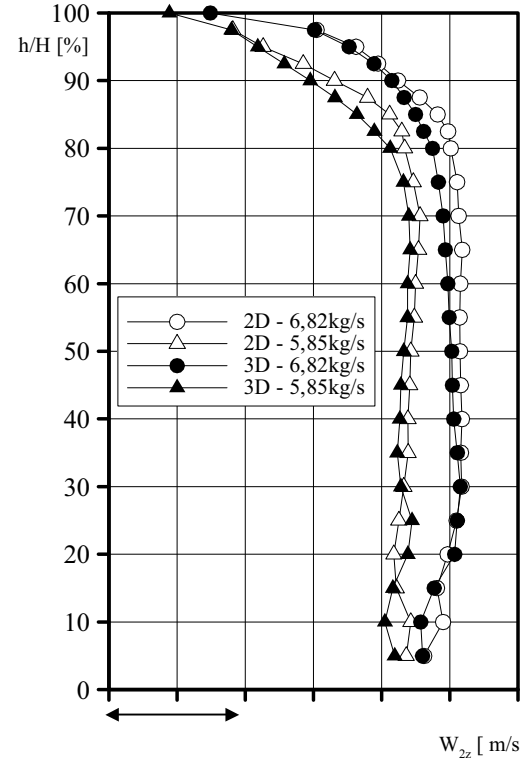

Figure 14: Measured averaged axial velocities of rotors 2D and 3D at design point and near stall

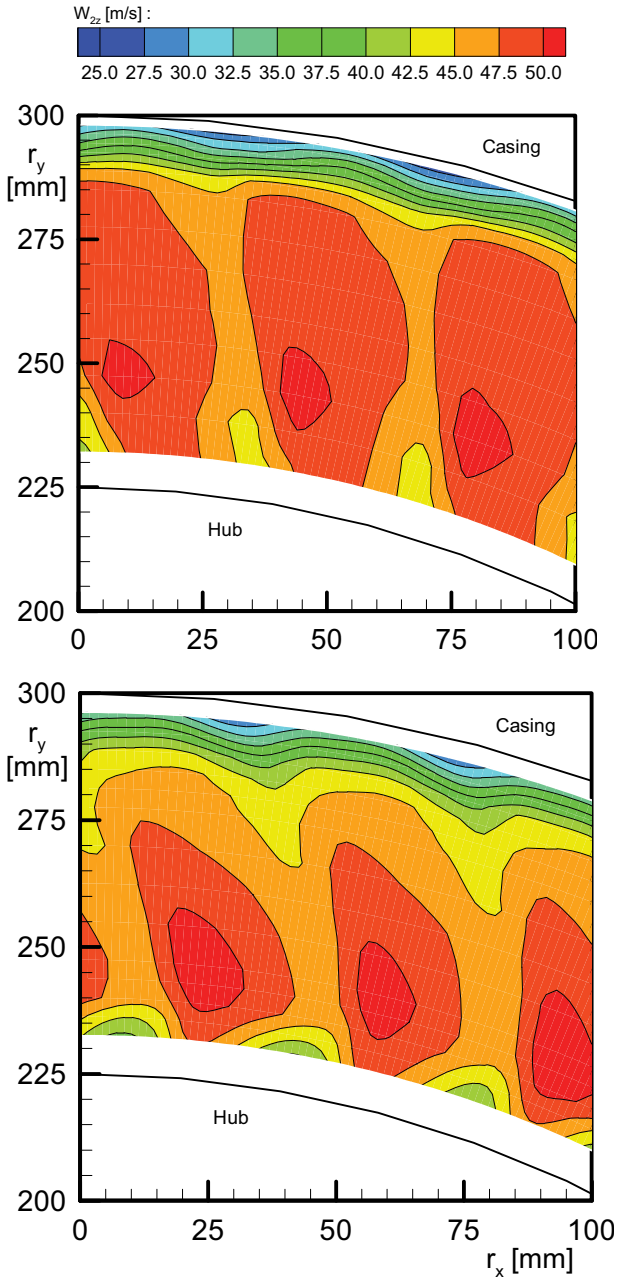

Figure 15: Measured axial velocities of rotors 2D and 3D at design point

The measured circumferentially averaged axial velocity distribution in Figure 14 corresponds with the calculated total pressure distributions in Figure 13, confirming the uniformization of the loading along blade height. This becomes also clear by the circumferentially resolved axial velocities in Figure 15. The axial velocities show a reduction of the values at blade mid height and an increase towards the rotor tip, the angles – not shown here – in contrast show an increase at mid height and a decrease towards the tip. These in combination yield to the described uniformization of the radial distributions. But the reason for the uniformization is hardly noticeable in Figure 15, since the measurement is not resolved sufficiently towards the end-walls. Only when the calculated circumferentially resolved axial velocities in Figure 16 are examined it

becomes clear: It confirms the improvement of the flow close to the hub and casing, which has been seen before in the losses (Figure 12). Already in the design point Figure 16 shows two effects: i) The size of the gap vortex, that means the region with very low axial velocity close to the casing is smaller for rotor 3D than for rotor 2D, ii) The region of small velocity at the suction side between hub and blade mid height, which points to a suction side separation or a weak boundary layer is for rotor 3D also smaller than for rotor 2D. This difference becomes even more obvious close to the stall margin. By the smaller blockage of the passage at rotor 3D, caused by the improved flow close to the end-walls, the flow is decelerated at mid height. But at the same time the measured distributions (Figures 15) show a velocity deficit at rotor 3D locally close to the hub for the design point and also for the near stall point, not shown here. This phenomenon can be explained by an under-turning of the flow.

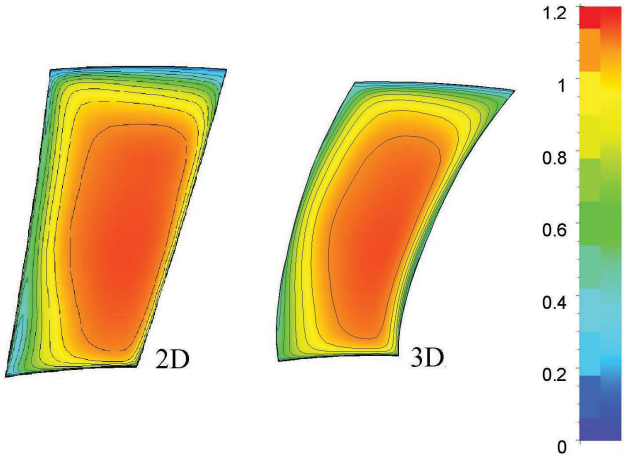

Figure 16: Calculated normalized axial velocities of rotors 2D and 3D at design point

5.3 3D-flow field at the casing

With the measured static pressure distributions at the casing above the rotor tip the behavior of the gap vortex of rotor 2D and 3D can be analysed. At the design point, Figure 17 shows a larger pressure minimum close to the leading edge regarding strength and size for rotor 2D. This is a strong driver for the formation of the gap vortex. The steepness of the vortex trajectory, shown as a white line, marked a), in Figure 17, is an indicator for the blockage generated by the vortex and for the stability margin of a tip critical rotor and hence a criterion for the stability of the vortex. Already at the design point the stability of rotor 2D is slightly smaller than of rotor 3D, since the inclination of the vortex trajectory is 5° smaller for rotor 3D. This behavior gets more pronounced when the compressor is throttled towards stall.

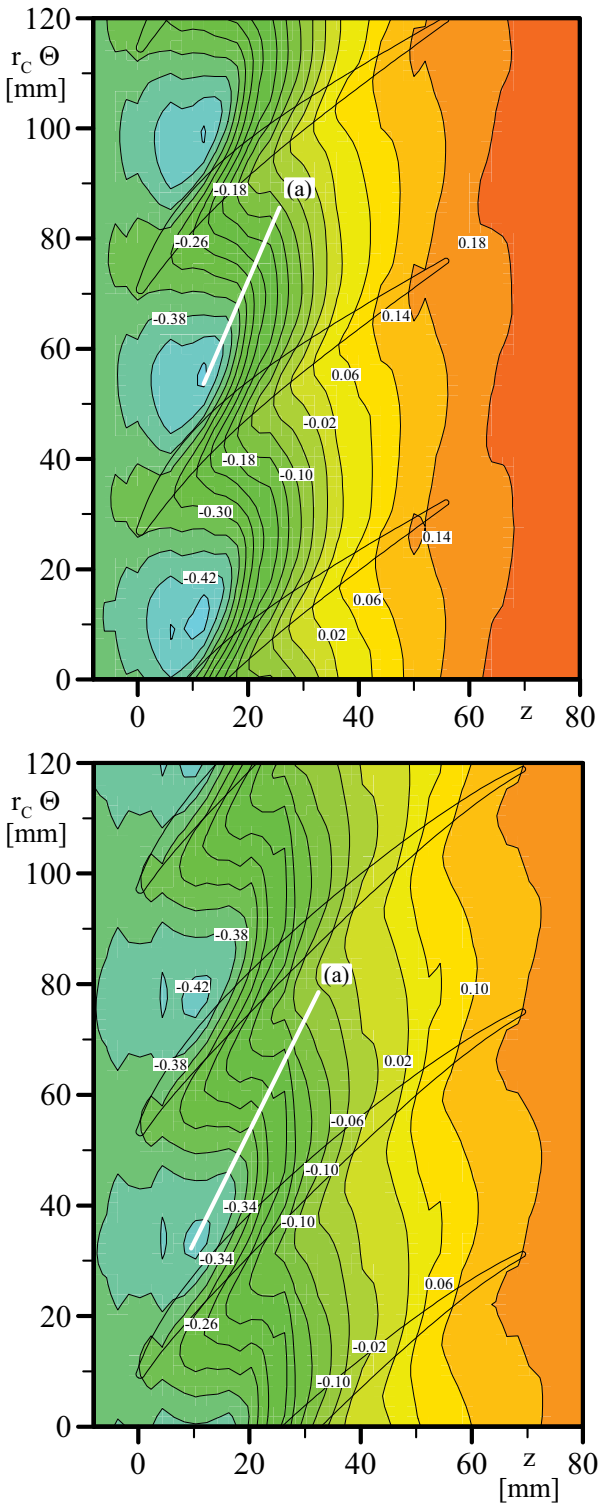

Figure 17: Measured static casing pressures for rotor 2D (top) and 3D (bottom) at the design point with vortex trajectory (a)

Even more concisely the behavior of the gap vortex can be explained by the comparison of the rotor casing flow, visualized with oil flow technique, and the corresponding calculated stream-lines on the casing in Figures 18 and 19.

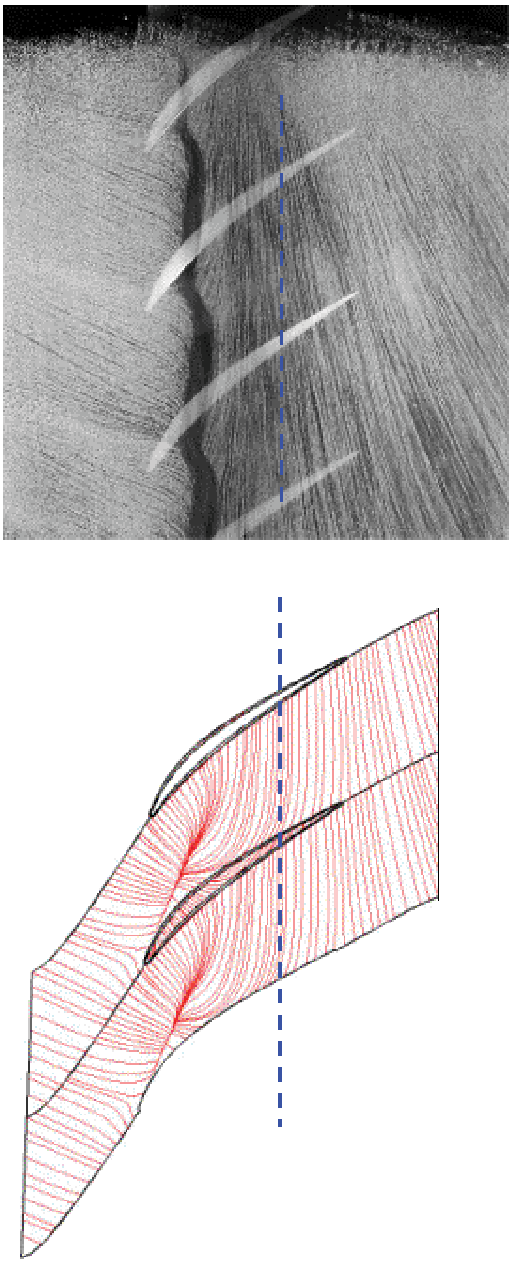

Figure 18: Oil flow visualization and calculated stream-lines at the casing of rotor 2D near stall with attachment line

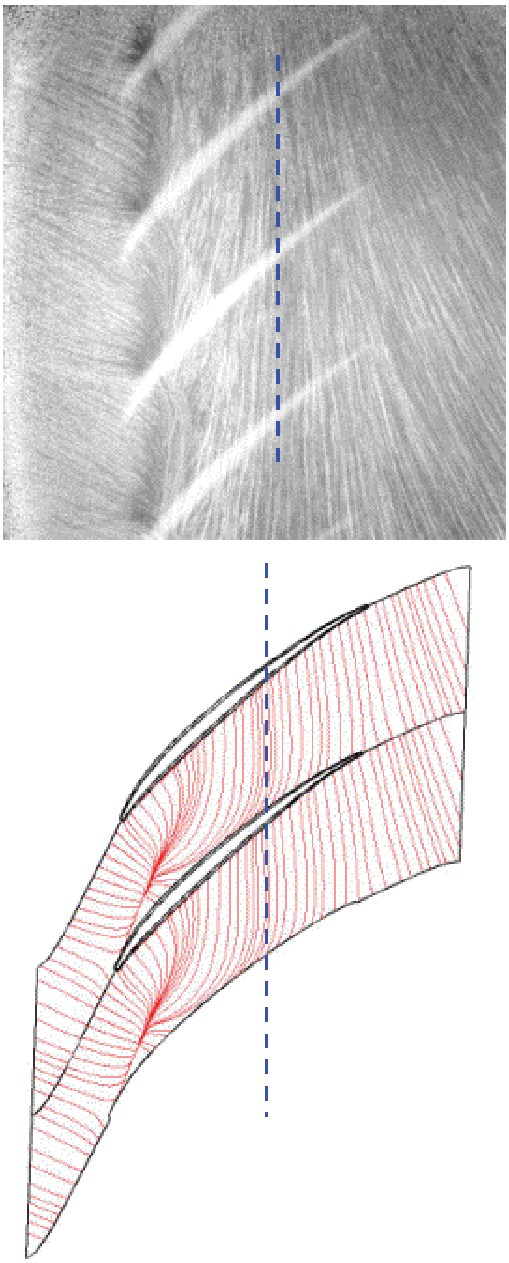

Figure 19: Oil flow visualization and calculated stream-lines at the casing of rotor 3D near stall with attachment line

For the design point (Figures 18 and 19) it can be seen for rotor 2D as well as for rotor 3D a good agreement of calculation and measurement, especially concerning the position of the attachment line (marked blue). It is for rotor 2D closer to the trailing edge and backs the observation from Figure 17, that the gap vortex of rotor 2D has less stability margin. This conclusion is also reinforced by the shape of the vortex. Especially the measurement shows, that the gap vortex of rotor 2D is significantly stronger, which can be seen on the oil film, which is smeared to a thick black band in the region where the vortex rolls-up. The smeared zone marks the position of the separation line.

It corresponds well with the point of the most pronounced 3D separation close to the vortex trajectory in the calculated stream-lines in Figures 18 and 19 and with the point of the largest suction pressure in the measured static casing pressures in Figure 17. The vortex strength at rotor 3D is much smaller, shown by the measured stream-lines, which are not smeared and hence show the vortex structure. Also this result agrees well with the calculated stream-lines, since the shape density and position of the calculated and measured stream-lines is similar. This confirms the statement, which has been made in the discussion of the static casing pressure distributions before.

6 SUMMARY AND CONCLUSIONS

The present paper describes the main features for a systematic three-dimensional method for the design of axial compressor blades. The method considers the application of sweep and dihedral as well as the three-dimensional inverse calculation of the radial camber-line distribution. With this new method, especially the aerodynamically critical regions close to the end-walls and the hub and tip gaps can be well adjusted to the flow. The primary goal of the introduction of the new design approach is to enhance compressor efficiency.

The parameter for the application of sweep and dihedral are derived with a parametric study. The study is carried out using a specially developed simple but three-dimensional panel method based on wing theory. With that panel method the three-dimensional load distribution of a blade with arbitrary geometry and shape can be determined.

For the inverse calculation of the radial camber-line distribution a second panel method is developed, which is based on the same approach as the first one, but it calculates the three-dimensional camber-line distribution for a given blade plan form and three-dimensional load distribution.

This new method enables a systematic aerodynamic design of a compressor blade [17]. To validate the method, a design for a highly-loaded rotor for a single-stage low-speed compressor is carried out. The three-dimensional designed blade has been manufactured and tested in the single-stage low-speed compressor rig of the *Pfleiderer*-Institute at the Technical University of Braunschweig. All results, experimental and numerical, are compared with those of a two-dimensional rotor – this means without sweep and dihedral – which has been optimised iteratively with modern CDA profiles.

The result is an improvement in efficiency of 0.5 % numerically and 1.1 % experimentally combined with an improvement in compressor stability.

In this paper only the application of the new method for compressor rotors is presented, but it is also possible to use the method for the three-dimensional design of compressor stators. The applicability of the method for stators has been demonstrated for a cantilevered stator for the four-stage low-speed compressor of the TU Dresden [18].

7 ACKNOWLEDGMENTS

The present work is part of the PhD thesis of C. Clemen, which has been performed with sponsorship of Rolls-Royce Deutschland Ltd. & Co. KG. Special thanks to U. Wenger, Prof. K. Vogeler and Prof. R. Radespiel for supporting the work.
The authors acknowledge the management of Rolls-Royce Deutschland Ltd. & Co. KG for the permission to publish this paper.

8 NOMENCLATURE

Abbreviations

2D	two-dimensional
3D	three-dimensional
AdComB	advanced compressor blading
AP	design point
CDA	controlled diffusion airfoil
CFD	computational fluid dynamics
HP	high-pressure
IGV	inlet guide vane
NS	near stall
RANS	Reynolds-averaged Navier-Stokes
SM	stall margin
TU	technical university

Parameters

α	angle of attack
Π	pressure ratio
η	efficiency, circumferential coordinate
φ	sweep angle
ν	dihedral angle
λ	stagger angle
θ	cirumferential angle
ξ	axial coordinate
ξ_{VR}	loss coefficient
ζ	radial coordinate
$\Delta x, \Delta y, \Delta z$	increment of axial, cirumferential and radial coordinate
h	local height
H	absolute height
kg	kilogram
l	chord length
mm	millimeter
$\dot{m}$	mass-flow
p	pressure
Pa	Pascal
r	radius
rpm	revolutions per minute
s	gap height
t	spacing
U	velocity
W	velocity
x	axial coordinate
y	circumferential coordinate
y^+	non-dimensional cell size
z	radial coordinate

Indices

∞	infinity
'	local
0	hub/casing
2	rotor exit plane
2D	two-dimensional
AP	design point
c	casing
MAX	maximum
tot	total
x, y, z	coordinates

9 REFERENCES

[1] Gümmer, V., Swoboda, M., Goller, M., Dobat, A., "The Impact of Rotor Tip Sweep on the Three-Dimensional Flow in a Highly-Loaded Single-Stage Low-Speed Axial Compressor, Part I: Design and Numerical Analysis", Proceedings of the 5th European Conference on Turbomachinery, Fluid Dynamics and Thermodynamics, Prague, Czech Republic, March 18.-21, pp. 163-174, 2003.

[2] Rohkamm, H., Wulff, D., Kosyna, G., Saathoff, H., Stark, U., Gümmer, V., Swoboda, M., Goller, M., "The Impact of Rotor Tip Sweep on the Three-Dimensional Flow in a Highly-Loaded Single-Stage Low-Speed Axial Compressor, Part II: Test Facility and Experimental Results", Proceedings of the 5th European Conference on Turbomachinery, Fluid Dynamics and Thermodynamics, Prague, Czech Republic, March 18.-21, pp. 175-186, 2003.

[3] Clemen, C., Gümmer, V., Goller, M., Rohkamm, H., Stark, U., Saathoff, H., "Tip-aerodynamics of forward swept rotor blades in a highly-loaded single-stage axial-flow low-speed compressor", ISROMAC 10-2004-027, The 10th of International Symposium on Transport Phenomena and Dynamics of Rotating Machinery, Honolulu, Hawaii, March 07-11, 2004.

[4] Goller, M., Gümmer, V., Clemen, C., Swoboda, Marius, „Enhancement of highly-loaded axial compressor stage performance using rotor blade tip tailoring;; Part I: Numerical design studies",Conference Proceedings, 6th European Conference on Turbomachinery, Lille, pp. 88-99, 2005

[5] Rohkamm, H., Kosyna, G., Saathoff, H., Stark, U., „Enhancement of highly-loaded axial compressor stage performance using rotor blade tip tailoring; Part II: Experimetal results",Conference Proceedings, 6th European Conference on Turbomachinery, Lille, pp. 100-110, 2005

[6] Bertin, J.J., Smith, M.L., „Aerodynamics for engineers", Prentice-Hall Inc., Englewood Cliffs, 1979

[7] Clemen, C., Stark, U., „Randeffekte in Axial-ventilatoren mit gesichelten Schaufeln", VDI-Report No. 1591 pp. 427-442, VDI Verlag, Düsseldorf, 2001

[8] Clemen, C., Stark, U., "Compressor blades with sweep and dihedral: A parameter study", 5th European Conference on Turbomachinery, Fluid Dynamics and Thermodynamics, Prague, Czech Republic, 18.-21. March, pp 151-162, 2003.

[9] Gallimore, Simon J., Bolger, John J., et al., „The use of sweep and dihedral in multistage axial flow compressor blading, Part I: University research and methods development", ASME GT-2002-30328, The American Society of Mechanical Engineering, New York, 2002

[10] Sasaki, T., Breugelmans, F., „Comparison of sweep and dihedral effects on compressor cascade performance", ASME 97-GT-2, The American Society of Mechanical Engineering, New York, 1997

[11] Kameier, F., Neise, W., „Reduction of tip clearance noise in axial-flow machines", AGARD-CP-571, pp. 13-1 – 13-12, Canada Communication Group, Hull, 1996

[12] Chen, G. T., „Vortical structures in turbomachinery tip clearance flows", Dissertation, Massachusetts Institute of Technology, Cambridge, 1991

[13] Stratford, B. S., „The prediction of separation of the turbulent boundary layer: An experimental flow with zero skin friction throughout its region of pressure rise", Journal of Fluid Mechanics, pp. 1-35, The American Society of Mechanical Engineering, 1959

[14] Friedrichs, J, Baumgarten, S., Kosyna, G., Stark, U., „Effect of stator design on stator boundary layer flow in a highly loaded single-stage axial-flow low-speed compressor", Proceedings of ASME Turbo Expo 2000 Paper 2000-GT-0616, The American Society of Mechanical Engineering, 1999

[15] Clemen, C., Stark, U., Friedrichs, J., Baumgarten, S., Kosyna, G., „Effect of mean line shape, sweep and dihedral on stator performance of a highly loaded single-stage axial-flow low-speed compressor", 6th European Conference on Turbomachinery, Fluid Dynamics and Thermodynamics, 7-11 March 2005, Lille, France, 2005

[16] Rohkamm, H., "Betriebsverhalten aerodynamisch hochbelasteter Axialverdichterstufen bei Modifikation der äusseren Schaufelenden im Rotor", PhD Thesis, Mitteilungen des Pfleiderer-Instituts für Strömungsmaschinen Vol. 11 January 2008, Verlag W. H. Faragallah, 2008

[17] Clemen, C., "Inverse camber-line calculation tool INCA-3D", Paper GT2008-50253, ASME Turbo Expo, Berlin, Germany, June 9-13, 2008.

[18] C. Clemen, H. Schrapp, V. Gümmer, R. Müller, M. Künzelmann, K. Vogeler, „Design of a highly-loaded four-stage low-speed research compressor", ASME GT 2008-50254, ASME Turbo Expo 2008, Berlin